LETTERS
https://doi.org/10.1038/s41563-022-01330-1

nature materials

Charge density waves in infinite-layer $NdNiO_2$ nickelates

Charles C. Tam[1,2,9], Jaewon Choi[1,9], Xiang Ding[3,9], Stefano Agrestini[1], Abhishek Nag[1,4], Mei Wu[5], Bing Huang[6], Huiqian Luo[7,8], Peng Gao[5], Mirian García-Fernández[1], Liang Qiao[3] ✉ and Ke-Jin Zhou[1] ✉

In materials science, much effort has been devoted to the reproduction of superconductivity in chemical compositions, analogous to cuprate superconductors since their discovery over 30 years ago. This approach was recently successful in realising superconductivity in infinite-layer nickelates[1–6]. Although differing from cuprates in electronic and magnetic properties, strong Coulomb interactions suggest that infinite-layer nickelates have a propensity towards various symmetry-breaking orders that populate cuprates[7–10]. Here we report the observation of charge density waves (CDWs) in infinite-layer $NdNiO_2$ films using Ni L_3 resonant X-ray scattering. Remarkably, CDWs form in Nd 5*d* and Ni 3*d* orbitals at the same commensurate wavevector (0.333, 0) reciprocal lattice units, with non-negligible out-of-plane dependence and an in-plane correlation length of up to ~60 Å. Spectroscopic studies reveal a strong connection between CDWs and Nd 5*d*–Ni 3*d* orbital hybridization. Upon entering the superconducting state at 20% Sr doping, the CDWs disappear. Our work demonstrates the existence of CDWs in infinite-layer nickelates with a multiorbital character distinct from cuprates, which establishes their low-energy physics.

The realisation of superconducting infinite-layer nickelates marks the latest milestone in the field of high-temperature superconductivity research[1–6]. Being isostructural to $CaCuO_2$, infinite-layer nickelates contain quasi-two-dimensional (2D) NiO_2 layers, nominal $3d^9$ Ni^{1+} ions with spin $S = 1/2$ and an active $d_{x^2-y^2}$ orbital near the Fermi level, analogous to the cuprate family of high-temperature superconductors[11]. However, X-ray absorption (XAS) and electron energy loss spectroscopies have shown that their electronic structure is closer to the Mott–Hubbard than the charge–transfer regime, distinct from cuprates[7,12]. Another distinctive feature in comparison with cuprates is that three-dimensional (3D) itinerant 5*d* bands of the rare-earth ions (*R* in $RNiO_2$) are predicted to hybridize with localized 2D Ni–O bands[7,11,13]. This strong hybridization is corroborated by resonant inelastic X-ray scattering (RIXS) where Nd 5*d*–Ni 3*d* hybridized states were observed[7], as well as a change in sign of the low-temperature Hall coefficient as a function of Sr doping, indicating the presence of two bands at the Fermi level[2,3].

On the other hand, although the magnetism of infinite-layer nickelates is under debate[14,15], $Nd_{1-x}Sr_xNiO_2$, grown on (and capped with) $SrTiO_3$ (STO), shows well-defined and highly dispersive magnetic excitations, validating the existence of strong electron Coulomb interactions in infinite-layer nickelates. In particular, this puts nickelates in proximity between strong antiferromagnetic (AFM) correlations and superconductivity[8]. Strong electronic and AFM correlations are key ingredients that give rise to symmetry-breaking orders, such as spin density waves (SDWs) or charge density waves (CDWs), which are relevant to superconductivity in cuprates[16]. A natural question is whether these ordered states are also present in infinite-layer nickelates. In this study we measured thin films of $NdNiO_2$ with Ni L_3-edge XAS and RIXS and revealed the presence of CDWs. We show that there is a clear correlation between CDWs and the hybridized Nd 5*d*–Ni 3*d* orbital, demonstrating the active participation of rare-earth 5*d* states in the low-energy physics of nickelates.

$Nd_{1-x}Sr_xNiO_2$ thin films ($NdNiO_2$ is 10 nm and Sr-doped $Nd_{1-x}Sr_xNiO_2$ is 15 nm) were prepared by pulsed laser deposition and subsequently topotactic reduction, similar to the methods applied in refs. [1,3] but without an STO-capping layer (Methods). We carried out structural analysis using X-ray diffraction (XRD), X-ray reflectivity (XRR), reciprocal space mapping (RSM) and rocking curve scans of the (002) diffraction peak, atomic force microscopy and scanning transmission electron microscopy (STEM; Methods and Supplementary Note 1). All thin films showed comparable crystalline quality, with a vast majority of the square-planar phase and a minor presence of the Ruddlesden–Popper (RP) secondary phase. The level of inhomogeneity (3.7 and 15.2% for the bulk and surface, respectively) was estimated from analysis of the O *K*-XAS spectra (Supplementary Note 2).

One of the reduced parent $NdNiO_2$ films, referred to as NNO_2-1 hereafter, features a two-peak Ni L_3 XAS profile consistent with those in $LaNiO_2$ and $NdNiO_2$ reported recently[7,17]. The first peak (denoted A') reflects the transition to the Nd 5*d*–Ni 3*d* hybridized states and the second peak (denoted A) detects the main absorption from $2p^6_{3/2}3d^9$ to $2p^5_{3/2}3d^{10}$ transition at the nominal Ni^{1+} sites (Fig. 1a,b)[7,17]. The O *K*-XAS spectra also show good consistency with other infinite-layer nickelates, in the bulk and surface of the film, namely the hole-peak weight is notably suppressed at the pre-edge owing to a much reduced O 2*p*–Ni 3*d* hybridization compared with pristine $NdNiO_3$ (Supplementary Note 4)[7,12,18].

To begin the search for symmetry-breaking orders, we performed momentum-dependent RIXS on NNO_2-1 (σ polarisation

[1]Diamond Light Source, Didcot, United Kingdom. [2]H. H. Wills Physics Laboratory, University of Bristol, Bristol, United Kingdom. [3]School of Physics, University of Electronic Science and Technology of China, Chengdu, China. [4]Laboratory for Non-linear Optics, Paul Scherrer Institut, Villigen, PSI, Switzerland. [5]International Center for Quantum Materials and Electron Microscopy Laboratory, School of Physics, Peking University, Beijing, China. [6]Beijing Computational Science Research Center, Beijing, China. [7]Beijing National Laboratory for Condensed Matter Physics, Institute of Physics, Chinese Academy of Sciences, Beijing, China. [8]Songshan Lake Materials Laboratory, Dongguan, Guangdong, China. [9]These authors contributed equally: Charles C. Tam, Jaewon Choi and Xiang Ding. ✉e-mail: liang.qiao@uestc.edu.cn; kejin.zhou@diamond.ac.uk

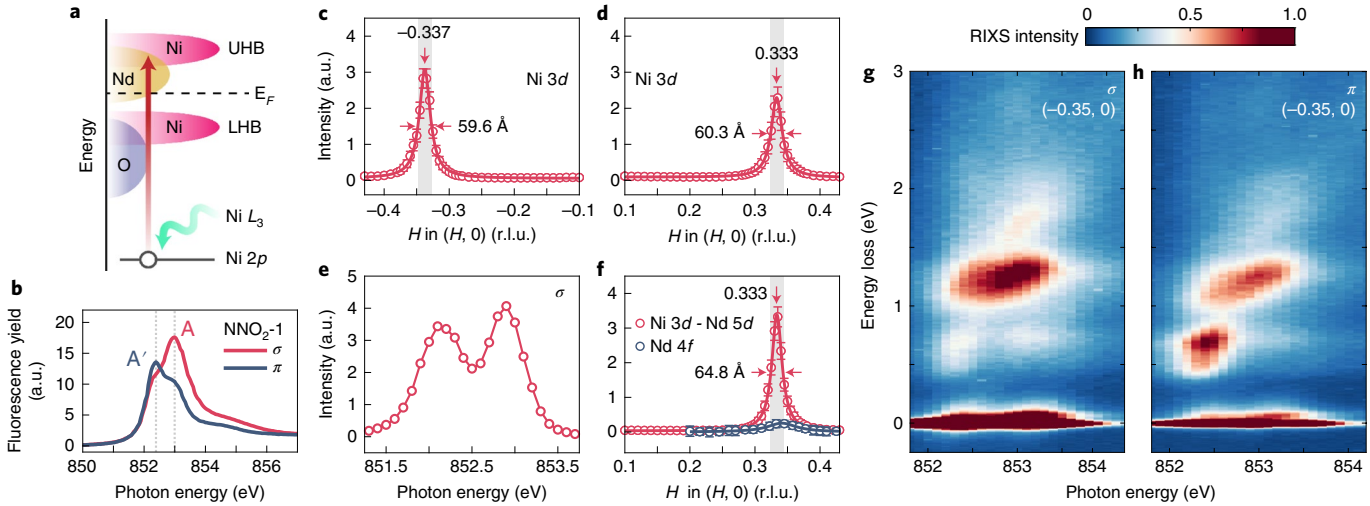

Fig. 1 | CDWs in the parent $NdNiO_2$ thin film NNO_2-1. a, Schematic electronic structure of infinite-layer nickelates. LHB (UHB) refers to lower (upper) Hubbard band. **b**, Ni L_3 XAS of the parent $NdNiO_2$ film NNO_2-1. **c**,**d**, Integrated quasi-elastic peak intensity as a function of momentum transfer along the $(\pm H, 0)$ direction by excitation at the Ni 3*d* resonance (A peak in **b**). The sign of the momentum transfer is defined in Methods (see also Supplementary Fig. 8). Fitted peak centre values are -0.337 ± 0.002 (**c**) and 0.333 ± 0.002 r.l.u. (**d**). Fitted correlation lengths are 59.6 ± 1.2 (**c**) and 60.3 ± 1.3 Å (**d**). **e**, The resonant energy profile of the CDW by fixing the momentum transfer to $Q_{CDW} = (+0.333, 0)$. **f**, Integrated quasi-elastic peaks as a function of momentum transfer along the $(H, 0)$ direction by probing the Ni 3*d*–Nd 5*d* hybridized state (A' peak in **b**) and Nd 4*f* states at the Nd M_5 edge. Fitted peak centre is 0.333 ± 0.002 r.l.u. and fitted correlation length is 64.8 ± 1.8 Å. **g**,**h**, RIXS maps with photon energy varied across the Ni L_3 edge on NNO_2-1 at 20 K at $H = -0.35$ r.l.u. with σ (**g**) or π incident X-ray polarisation (**h**). a.u. refers to arbitrary units.

was used throughout unless otherwise stated). By exciting at the Ni L_3 resonance peak (A in Fig. 1b), quasi-elastic scattering peaks appeared at $q_{\parallel} = -0.337 \pm 0.002$ and $q_{\parallel} = 0.333 \pm 0.002$ reciprocal lattice units (r.l.u.) along the primary direction $(H, 0)$—that is, the Ni–O bonding direction (Fig. 1c,d). Scanning in the (H, H) direction, however, did not reveal such peaks (Supplementary Fig. 9). To clarify the origin of the scattering peak, we fixed $q_{\parallel}$ to +0.333 r.l.u. and swept the incident photon energy across the Ni L_3 absorption edge. Interestingly, a pronounced double-resonance profile was found coinciding with the two absorption peaks (Fig. 1e). Photon energy scans at $q_{\parallel} = -0.35$ r.l.u. across the Ni L_3 revealed a much stronger signal with σ than with π polarisation. Likewise, the quasi-elastic peak in momentum space had the same polarisation dependence as charge excitations and opposite to that of spin excitations in cuprates (Supplementary Figs. 11 and 12)[10]. In addition, momentum-dependent RIXS scans off-tuned from the Ni L_3 resonance peak, taken at 840 eV, returned negligible quasi-elastic peaks (Supplementary Fig. 9). The above results suggest that the observed quasi-elastic scattering peak may be attributed to translational symmetry breaking induced by a charge density modulation. While there is potential contribution from a structural modulation or the defect phase to the quasi-elastic peak, we continue to refer to the phenomenon as CDW and discuss these possibilities later. Notably, double-resonance behaviour contrasts with the CDWs in cuprates where typically a singular resonance profile exists at the Cu L_3 edge[19].

Density-functional theory studies on infinite-layer nickelates uncovered sizable Ni $3d_{3z^2-r^2}$ mixing with the rare-earth $5d_{3z^2-r^2}$ and $5d_{xy}$ states, leading to 3D Fermi surface pockets that slightly hole dope the half-filled Ni $3d_{x^2-y^2}$ band[11,13,20]. As a result, Ni $3d_{3z^2-r^2}$ weight appears near the Fermi level although the Ni $3d_{3z^2-r^2}$ orbital is furthest away from the Ni $3d_{x^2-y^2}$ orbital in a simplified ligand field picture. The pre-peak in the Ni L_3 XAS spectra, as well as the ~0.6 eV energy loss feature in RIXS acquired in both σ and π polarisations, are signatures of the hybridized Nd 5*d*–Ni 3*d* orbitals containing $5d_{3z^2-r^2}$- and $5d_{xy}$-symmetries unique to infinite-layer nickelates (Fig. 1b,g,h). We thus positioned photon energy at the Ni–Nd hybridized states (A' in Fig. 1b) and scanned along the $(H, 0)$ direction. Remarkably, a quasi-elastic scattering peak appeared at the same wavevector as those at the Ni 3*d* resonance (Fig. 1f). Moreover, the quasi-elastic CDW peaks at Nd and Ni resonances show a comparable half-width at half-maximum (HWHM) $\Gamma = 0.01 \pm 0.002$ r.l.u. We define the in-plane correlation length $\xi_H = 1/\Gamma$, which corresponds to 60.3 ± 1.3 Å (Fig. 1c–f). The above results indicate that both Nd 5*d* and Ni 3*d* valence charges form density waves in NNO_2-1 propagating with the same period. A quasi-elastic scattering peak also appears at $q_{\parallel} = 0.340 \pm 0.004$ r.l.u. with excitation at the Nd M_5 edge (Fig. 1f). This substantially weakened intensity suggests that the localized 4*f* states are much less involved in the valence band near the Fermi level[7].

To explore the properties of CDWs in infinite-layer $NdNiO_2$, we designed a series of $NdNiO_2$ thin films by tuning the annealing temperature (Methods). Figure 2a–h summarizes the Ni L_3 XAS of the two new $NdNiO_2$ (denoted as NNO_2-2 and NNO_2-3, hereafter) together with that of NNO_2-1. The two-peak structure is clearly present in all XAS spectra projected along the in-plane, I_{ab}, and out-of-plane direction, I_c (Methods). Considering $NdNiO_2$ as a nominal d^9 system, we fitted the two peaks of the projected XAS spectra from which Nd 5*d* and Ni 3*d* orbital occupancy can be extracted (Methods). The Nd $5d_{3z^2-r^2}$ and Ni $3d_{3z^2-r^2}$ orbital content is thus the $I_c/(I_c + I_{ab})$. Figure 2m,n shows that both the Nd $5d_{3z^2-r^2}$ and Ni $3d_{3z^2-r^2}$ orbital contents decrease progressively, signalling reduced Nd–Ni hybridization from NNO_2-1 to NNO_2-3. The same monotonic trend was found for the surface layers of the samples (Supplementary Fig. 15). Conversely, the O*K*-XAS spectra were consistent across the three samples from the bulk and surface layers (Supplementary Note 4). RIXS maps of NNO_2-2 and NNO_2-3 also manifest qualitatively the same *dd* excitations as those in NNO_2-1 (Supplementary Note 3). The consistent bulk and surface spectroscopic results among all $NdNiO_2$ films suggest that the variation in Nd–Ni hybridization is a property of the majority square-planar phase rather than the minor RP defect phase.

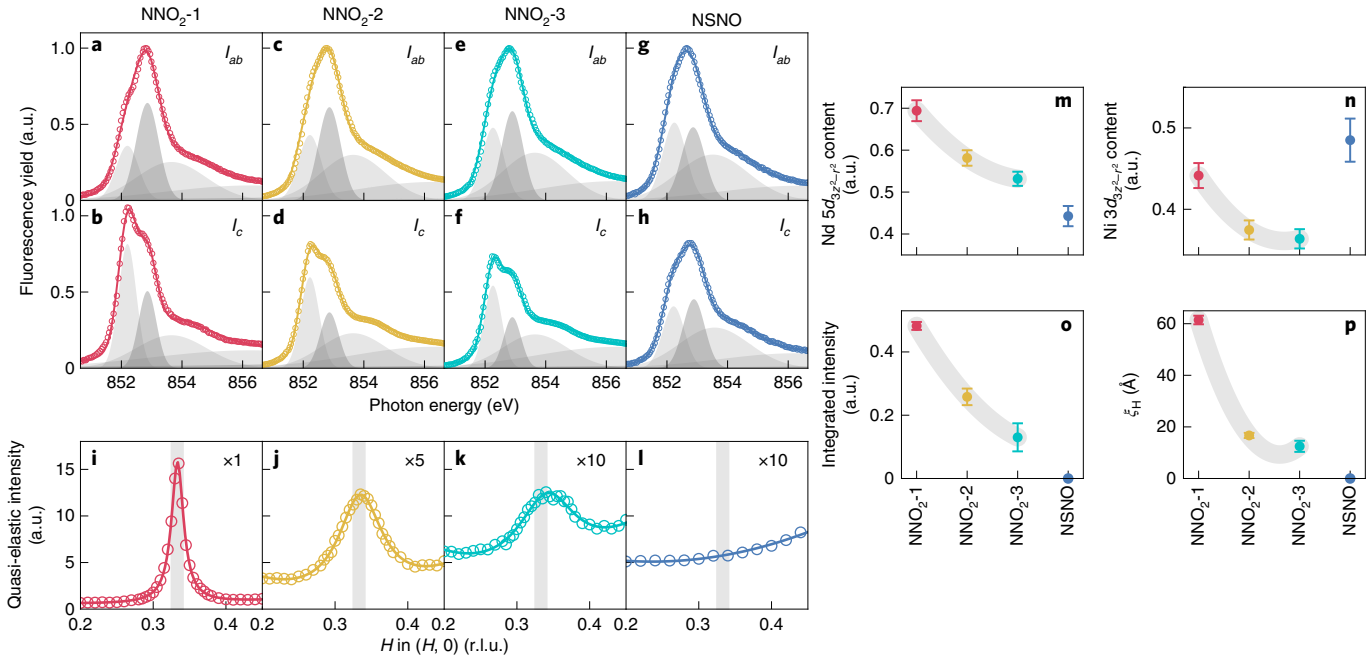

Fig. 2 | Nd 5*d*–Ni 3*d* orbital hybridization and CDW in $NdNiO_2$ and superconducting $Nd_{0.8}Sr_{0.2}NiO_2$. a–h, XAS projected in (out of) the NiO_2 planes, I_{ab} (**a**,**c**,**e**,**g**) (I_c) (**b**,**d**,**f**,**h**), of NNO_2-1 (**a**,**b**), NNO_2-2 (**c**,**d**), NNO_2-3 (**e**,**f**) and NSNO (**g**,**h**). The fit components visible in this energy range are plotted in different shades of grey (fitting details provided in Methods). **i**–**l**, Quasi-elastic peak intensity showing a CDW plotted in the three $NdNiO_2$ films with y axis scaled ×1, (**i**), ×5 (**j**) and ×10 (**k**), with no evidence of CDW in NSNO (**l**). The Nd $5d_{3z^2-r^2}$ orbital content (**m**), Ni $3d_{3z^2-r^2}$ orbital content (**n**), CDW integrated intensity (**o**) and CDW in-plane correlation length (**p**) show similar trends for the $NdNiO_2$ samples. Error bars are from least-squares fitting.

Figure 2i–l summarizes the integrated quasi-elastic peak intensities as a function of $q_{\parallel}$ along the $(H,0)$ direction, showing clearly CDWs in all $NdNiO_2$ samples. To make a quantitative assessment, we compare the fitted CDW intensity and in-plane correlation length. Figure 2o,p shows monotonically decreasing CDW integrated intensity and in-plane correlation length, respectively, from NNO_2-1 to NNO_2-3. A similar trend was found between CDWs and the $d_{3z^2-r^2}$ orbital content across the three parent $NdNiO_2$, suggesting that CDWs may hold an intimate connection with Nd–Ni hybridization (Fig. 2m,n). Notably, the CDWs in $NdNiO_2$ are commensurate, propagating along the Ni–O bonding direction, distinct from the charge order formed along the Ni–Ni bonding direction in both single-layer $La_{2-x}Sr_xNiO_4$ and trilayer $La_4Ni_3O_8$ nickelates[21,22].

We also studied a superconducting $Nd_{0.8}Sr_{0.2}NiO_2$ film, with superconducting transition temperature $T_c = 10$ K (referred to as NSNO hereafter). XAS and RIXS measurements were conducted under the same experimental geometry. Whereas NSNO presents similar O *K*-XAS spectra compared with the parent samples (Supplementary Note 4), the Ni L_3 I_c XAS changed markedly in that the Nd resonance peak became much reduced. In comparison with the parent samples, the Nd $5d_{3z^2-r^2}$ orbital content decreases sharply, indicating that Nd–Ni hybridization is further reduced in the superconducting sample (Fig. 2m). This is in line with the fact that 20% Sr doping depletes most of the itinerant Nd 5*d* electron carriers[2,3]. The Ni $3d_{3z^2-r^2}$ orbital content increases, deviating from the trend in both bulk and surface (Fig. 2n and Supplementary Fig. 14), which suggests that the orbital character became more isotropic than in $NdNiO_2$, which supports the premise that Ni states become more d^8-like. Interestingly, no CDW signals were detected along either the $(H,0)$ or (H,H) direction (Fig. 2l and Supplementary Fig. 9). The results for both parent and superconducting samples suggest that the Nd 5*d* hybridized orbital actively contributes to CDW ordered states in infinite-layer nickelates. The situation is disparate to cuprates, where conventional CDWs are normally hosted in the CuO_2 layers rather than in the spacer-layers, and are quasi-two dimensional[10,23].

To further explore the properties of CDWs in infinite-layer nickelates, we examined L dependence, that is the momentum dependence out of the NiO_2 plane. In Fig. 3a,b are plotted a series of CDW scans peaked at $(0.333, 0, L)$ from both NNO_2-1 and NNO_2-2, where L was changed discretely (Methods). Notably, the integrated CDW intensity (Fig. 3c,d) and peak width (Fig. 3e,f) changes substantially when L is decreased from 0.34 to 0.27. Due to the limit of Ni L_3 resonance energy and a relatively short *c*-axis lattice parameter, only a very small portion of the L space is accessible. Nevertheless, the non-negligible L dependence implies that CDWs may have a 3D nature. Further studies using hard X-ray scattering may shed light on the question of dimensionality.

Finally, we performed temperature-dependent RIXS measurements to understand the characteristic temperature of the CDW. Figure 4a,b displays staggered CDW peaks of NNO_2-1 and NNO_2-2, respectively. Although temperature-dependent CDW intensities decayed exponentially, from which a critical T_{CDW} was obtained (Fig. 4c), no substantial change was seen for in-plane correlation length (Fig. 4d). With increasing temperature, the CDW intensity decayed to a persistent non-zero intensity up to 300 K, similar to dynamical CDW fluctuations in cuprates[24,25]. It is remarkable that the stronger CDWs retained a relatively high characteristic temperature, T_{CDW}, as illustrated in Fig. 4e. The unconventional nature of CDWs is also implied by previously published data, since neither a resistivity anomaly nor a structural phase transition was seen[1]. This is in contrast to long-range quasi-static CDWs found in the stripe phase of nickelates, or in classical linear-chain compounds[21,22,26].

The growth of nickelate superconductors is challenging due to their unstable chemical form and susceptibility to structural defects. Thus, it is essential to determine whether the phenomena we see are genuine rather than a byproduct of growth. The structural analysis of our films reveals a minor contribution of RP defects compared

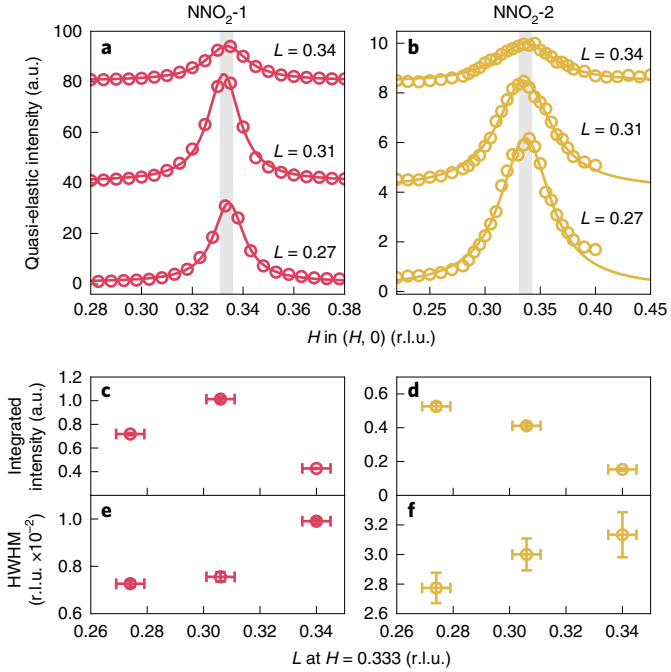

Fig. 3 | *L* dependence of CDW in $NdNiO_2$. **a**,**b**, Integrated quasi-elastic peaks and their Lorentzian fits along the (*H*, 0) direction with each acquired at a different Ω value for NNO_2-1 (**a**) and NNO_2-2 (**b**). Ω was chosen such that CDW scattering peaked at $H = 0.333$, with the corresponding *L* value labelled. Measurements at successively higher *L* values have been offset for clarity. **c**,**d**, Integrated intensity of CDW peak as a function of *L* at $H = 0.333$ for NNO_2-1 (**c**) and NNO_2-1 (**d**). **e**,**f**, CDW peak width (HWHM) as a function of *L* for NNO_2-1 (**e**) and NNO_2-1 (**f**). **c**–**f**, Error bars for intensity and width are from least-squares fitting, while horizontal error bars represent momentum resolution at the Ni L_3 RIXS.

with a vast majority of the infinite-layer phase, despite a small difference in lattice constants (Supplementary Table 1). The O *K*-XAS pre-edge spectra also suggest that the infinite-layer phase dominates in thin films. However, a minor degree of defects and the possible intercalation of hydrogen onto apical sites may vary in $NdNiO_2$ films, given that they underwent topotactic reduction under different temperatures. Although the consistent Q_{CDW} across three unique $NdNiO_2$ films indicates that these defects are unlikely to be the main cause of the symmetry-breaking order, more systematic studies are required to obtain a full picture of the origin. Regarding the case of structural modulation of Nd and Ni cations, although there is no obvious hint from structural analysis that this is the case, it may be induced by a charge modulation via electron–phonon coupling[21,23]. It is interesting to note that a previous RIXS study on STO-capped $NdNiO_2$ films did not reveal any CDW signals, but rather magnons, while in the current work on non-capped $NdNiO_2$ we saw robust CDWs without sizeable magnetic excitations (Supplementary Fig. 11)[8]. These contradictory results suggest that STO-capping layers may influence $NdNiO_2$ beyond simple surface protection, and indicate the need for systematic investigation.

So far we have experimentally confirmed the existence of CDWs in infinite-layer $NdNiO_2$ films. More importantly, the involvement of Nd $5d_{xy}$, Nd $5d_{3z^2-r^2}$ and Ni $3d_{x^2-y^2}$ orbitals in the formation of CDWs clearly demonstrates that a minimal multiorbital model is required to describe the low-energy physics of infinite-layer nickelates[11,13,20]. In cuprates, low-energy physics is mostly captured by a single hybridized Cu 3*d* and O 2*p* orbital within the CuO_2 planes, although it has been shown that a multiorbital model is required[19]. Also, unlike CDWs prevalent in optimally or underdoped cuprates[23], CDWs are persistent in the parent infinite-layer $NdNiO_2$ films. Although this, at first sight, may seem incompatible with the half-filling condition, the parent compound is slightly self-doped and metallic, effectively mimicking a very underdoped state[7,11,13]. A broader question is whether CDWs in infinite-layer nickelates are intertwined with other symmetry-breaking orders, such as AFM order, SDW or the superconducting state, as in cuprates[16]. The missing AFM order may be connected to the competition with the robust CDW state, although the exact cause is yet to be explored[14]. Concerning the relationship between CDWs and superconductivity, our studies are insufficient to be able to make a definitive conclusion but no CDWs were seen in superconducting $Nd_{0.8}Sr_{0.2}NiO_2$. Future studies on Sr-doped $Nd_{1-x}Sr_xNiO_2$ with different carrier concentrations are desired. More speculatively, the involvement of Nd $5d_{3z^2-r^2}$ and Ni $3d_{x^2-y^2}$ orbitals close to the Fermi level resembles the situation in some cuprates where the contribution from Cu $3d_{3z^2-r^2}$ orbital works against superconductivity[27,28]. If the Nd 5*d* states are deemed crucial for low-energy physics, CDWs may appear more competing with, than cooperative to, superconductivity.

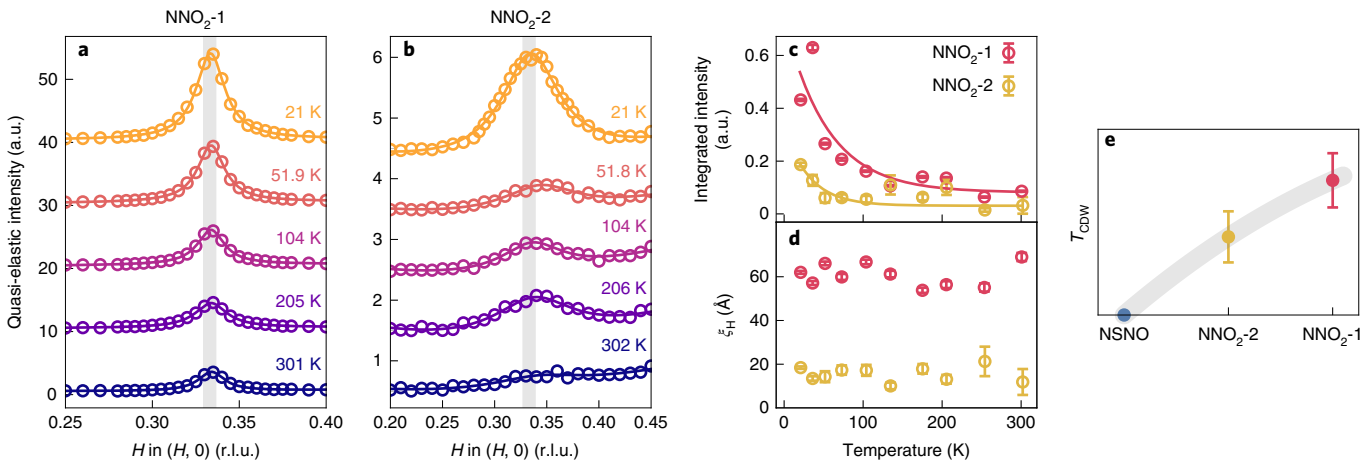

Fig. 4 | Temperature dependence of CDW in $NdNiO_2$. **a**,**b**, CDW peaks and their Lorentzian fits along the (*H*, 0) direction at various temperatures for NNO_2-1 (**a**) and NNO_2-2 (**b**). **c**, Integrated CDW intensity as a function of increased temperature. Temperature dependence is fitted with an exponential function (Methods). **d**, CDW in-plane correlation length as a function of increased temperature. **e**, For a relative comparison, the characteristic CDW temperature is defined as the temperature at which CDW intensity is $1/e^2$ for NSNO, NNO_2-2 and NNO_2-1. **c**–**e**, Error bars are from least-squares fitting.

Note: similar works on other infinite-layer nickelates appeared at the time of submission of this article[29,30]

Online content

Any methods, additional references, Nature Research reporting summaries, source data, extended data, supplementary information, acknowledgements, peer review information; details of author contributions and competing interests; and statements of data and code availability are available at https://doi.org/10.1038/s41563-022-01330-1.

Received: 8 December 2021; Accepted: 7 July 2022;
Published online: 18 August 2022

References

1. Li, D. et al. Superconductivity in an infinite-layer nickelate. *Nature* **572**, 624–627 (2019).
2. Li, D. et al. Superconducting dome in $Nd_{1-x}Sr_xNiO_2$ infinite layer films. *Phys. Rev. Lett.* **125**, 027001 (2020).
3. Zeng, S. et al. Phase diagram and superconducting dome of infinite-layer $Nd_{1-x}Sr_xNiO_2$ thin films. *Phys. Rev. Lett.* **125**, 147003 (2020).
4. Osada, M., Wang, B. Y., Lee, K., Li, D. & Hwang, H. Y. Phase diagram of infinite layer praseodymium nickelate $Pr_{1-x}Sr_xNiO_2$ thin films. *Phys. Rev. Mater.* **4**, 121801 (2020).
5. Osada, M. et al. Nickelate superconductivity without rare-earth magnetism: $(La,Sr)NiO_2$. *Adv. Mater.* **33**, 2104083 (2021).
6. Zeng, S. et al. Superconductivity in infinite-layer lanthanide nickelates. *Sci. Adv.* **8**, eabl9927 (2022).
7. Hepting, M. et al. Electronic structure of the parent compound of superconducting infinite-layer nickelates. *Nat. Mater.* **19**, 381–385 (2020).
8. Lu, H. et al. Magnetic excitations in infinite-layer nickelates. *Science* **365**, 213–216 (2021).
9. Tranquada, J., Sternlieb, B., Axe, J., Nakamura, Y. & Uchida, S. Evidence for stripe correlations of spins and holes in copper oxide superconductors. *Nature* **375**, 561–563 (1995).
10. Ghiringhelli, G. et al. Long-range incommensurate charge fluctuations in $(Y,Nd)Ba_2Cu_3O_{6+x}$. *Science* **337**, 821–825 (2012).
11. Lee, K.-W. & Pickett, W. Infinite-layer $LaNiO_2$: Ni^{1+} is not Cu^{2+}. *Phys. Rev. B* **70**, 165109 (2004).
12. Goodge, B. H. et al. Doping evolution of the Mott–Hubbard landscape in infinite-layer nickelates. *Proc. Natl Acad. Sci. USA* **118**, e2007683118 (2021).
13. Been, E. et al. Electronic structure trends across the rare-earth series in superconducting infinite-layer nickelates. *Phys. Rev. X* **11**, 011050 (2021).
14. Hayward, M. & Rosseinsky, M. Synthesis of the infinite layer Ni (I) phase $NdNiO_{2+x}$ by low temperature reduction of $NdNiO_3$ with sodium hydride. *Solid State Sci.* **5**, 839–850 (2003).
15. Yi, C. et al. NMR evidence of antiferromagnetic spin fluctuations in $Nd_{0.85}Sr_{0.15}NiO_2$. *Chin. Phys. Lett.* **38**, 067401 (2021).
16. Fradkin, E., Kivelson, S. A. & Tranquada, J. M. Colloquium: theory of intertwined orders in high temperature superconductors. *Rev. Mod. Phys.* **87**, 457 (2015).
17. Rossi, M. et al. Orbital and spin character of doped carriers in infinite-layer nickelates. *Phys. Rev. B* **104**, L220505 (2021).
18. Chen, Z. et al. Electronic structure of superconducting nickelates probed by resonant photoemission spectroscopy. *Matter* **6**, 1806–1815 (2022).
19. Li, J. et al. Multiorbital charge-density wave excitations and concomitant phonon anomalies in $Bi_2Sr_2LaCuO_{6+\delta}$. *Proc. Natl Acad. Sci. USA* **117**, 16219–16225 (2020).
20. Sakakibara, H. et al. Model construction and a possibility of cupratelike pairing in a new d^9 nickelate superconductor (Nd, Sr)NiO_2. *Phys. Rev. Lett.* **125**, 077003 (2020).
21. Cheong, S.-W. et al. Charge-ordered states in $(La, Sr)_2NiO_4$ for hole concentrations n_h=1/3 and 1/2. *Phys. Rev. B* **49**, 7088 (1994).
22. Zhang, J. et al. Stacked charge stripes in the quasi-2D trilayer nickelate $La_4Ni_3O_8$. *Proc. Natl Acad. Sci. USA* **113**, 8945–8950 (2016).
23. Comin, R. & Damascelli, A. Resonant X-ray scattering studies of charge order in cuprates. *Annu. Rev. Condens. Matter Phys.* **7**, 369–405 (2016).
24. Miao, H. et al. High-temperature charge density wave correlations in $La_{1.875}Ba_{0.125}CuO_4$ without spin–charge locking. *Proc. Natl Acad. Sci. USA* **114**, 12430–12435 (2017).
25. Arpaia, R. et al. Dynamical charge density fluctuations pervading the phase diagram of a Cu-based high-T_c superconductor. *Science* **365**, 906–910 (2019).
26. Grüner, G. The dynamics of charge-density waves. *Rev. Mod. Phys.* **60**, 1129 (1988).
27. Sakakibara, H., Usui, H., Kuroki, K., Arita, R. & Aoki, H. Two-orbital model explains the higher transition temperature of the single-layer Hg-cuprate superconductor compared to that of the La-cuprate superconductor. *Phys. Rev. Lett.* **105**, 057003 (2010).
28. Peng, Y. et al. Influence of apical oxygen on the extent of in-plane exchange interaction in cuprate superconductors. *Nat. Phys.* **13**, 1201–1206 (2017).
29. Rossi, M. et al. A broken translational symmetry state in an infinite-layer nickelate. *Nat. Phys.* https://www.nature.com/articles/s41567-022-01660-6 (2022).
30. Krieger, G. et al. Charge and spin order dichotomy in NdNiO2 driven by the capping layer. *Phys. Rev. Lett.* **129**, 027002 (2022).

Methods

Thin film growth. Perovskite $NdNiO_3$ thin films (10 nm) were grown on TiO_2-terminated STO (001) substrates by pulsed laser deposition using a 248 nm KrF excimer laser. Before deposition, solid-state targets were prepared by sintering and pelletizing stochiometric mixtures of NiO and Nd_2O_3 powder at 1,300 °C for 12 h. The perovskite $Nd_{0.8}Sr_{0.2}NiO_3$ thin film is 15 nm thick and was grown using the same laser parameters as for $NdNiO_3$ thin films. Solid-state targets were prepared by sintering and pelletizing stochiometric mixtures of NiO, Nd_2O_3 and $SrCO_3$ powder at 1,300 °C for 12 h (ref. [31]). During deposition, a laser fluence of 1.2 J cm^{-2} was used to ablate the target; the substrate temperature was controlled at 620 °C with an oxygen pressure of 200 mTorr. No samples had STO-capping layers. After growth, the thin films were cooled to room temperature under the same oxygen environment.

Extra care was paid to the growth of perovskite $Nd_{0.8}Sr_{0.2}NiO_3$ thin films. This is because Sr doping makes the growth of the films more difficult to control than their parent counterpart due to the inclination towards island or layer-island growth rather than epitaxial growth. High-quality, layer-by-layer growth is necessary to minimize the level of the defect phases present to achieve superconductivity[32].

Perovskite samples were reduced to the infinite-layer phase by following a topotactic reduction method similar to that detailed in ref. [1]. The perovskite films were vacuum-sealed (<0.1 mTorr) together with 0.1 g of solid-state CaH_2 powder. The temperature profile of the reduction procedure followed a trapezoidal shape. Warming and cooling rates were held at 10 °C min^{-1}. On the plateau, reduction was held at a steady temperature for an optimized time of 2 h. Reduction temperatures of 200, 220 and 290 °C were used to produce the $NdNiO_2$ films denoted NNO_2-1, NNO_2-3 and NNO_2-2, respectively. The $Nd_{0.8}Sr_{0.2}NiO_3$ sample was reduced for 2 h at an optimized temperature of 300 °C. $NdNiO_2$ films crystallize tetragonally and are assumed to have in-plane lattice parameters equivalent to STO $a=b=3.91$ Å. The c lattice parameters were obtained by XRD (Supplementary Note 1).

Thin film characterization. Reflection high-energy electron diffraction with a 15 keV electron beam was used to monitor film quality during growth. Resistivity was measured by a four-probe method via wire-bonded contacts in a cryogen-free magnet system (CFMS, Cryogenic) down to 1.6 K. XRR, atomic force microscopy, rocking curve scans and RSM of the (002) diffraction peak, and STEM were used to characterize the thin films. XRR, RSM and XRD measurements were performed using a monochromatic source of Cu Kα_1 (Bruker D8 Discover). Film surface morphology and roughness were examined by atomic force microscopy (NX-10, Park Systems). Atomic-resolution HAADF–STEM measurements were performed using an aberration-corrected FEI Titan Themis G2 at 300 kV. STEM specimens were first thinned by mechanical polishing and then subjected to argon ion milling. The ion milling process was carried out using a PIPS (Model 691, Gatan). The results of this characterization are detailed in Supplementary Note 1.

XAS and RIXS measurement. XAS and RIXS measurements were performed at Beamline I21, Diamond Light Source, UK[33]. The crystallographic a–c (or equivalently b–c) planes of all samples were aligned within the horizontal scattering plane (Supplementary Fig. 8). r.l.u. are defined (where $2\pi/a=2\pi/b=2\pi/c=1$) as $\boldsymbol{Q}=H\boldsymbol{a}^*+K\boldsymbol{b}^*+L\boldsymbol{c}^*$. For all data presented throughout, except for scans in (H,H), samples were aligned such that $K=0$. The polar angular offsets (θ and χ) of the films were aligned by specular reflection, and the azimuthal offset (ϕ) by CDW peak, such that the c^* axis was in the scattering plane. The spectrometer arm was at a fixed position of $\Omega=154°$, unless otherwise stated.

XAS spectra were collected with a grazing incidence angle of $\theta_0=20°$ to probe both in- and out-of-plane unoccupied states. All measurements were done at a temperature of 20 K with the exit slit opening to 50 μm at the Ni L_3 edge, except for temperature-dependent studies. Fluorescence yield XAS spectra were collected with a photodiode and normalized to incoming beam intensity. Both linear vertical (σ) and horizontal (π) polarisations were used. While σ-polarised light probes only in-plane XAS—that is, $I_{ab}=I_\sigma$—out-of-plane XAS were obtained by a combination of both σ and π polarisations with $I_c=\left(I_\pi-I_\sigma\sin^2[\theta_0]\right)/\cos^2[\theta_0]$.

Energy-dependent RIXS measurements were performed at an in-plane position of $Q=(-0.35,0)$ at a temperature of 20 K, with the exit slit opening to 30 μm corresponding to an average energy resolution of 41 meV (FWHM). The incident energy range was 851.5–854 eV, in steps of 100 meV, to fully capture resonance behaviour across Ni L_3 absorption peaks.

Momentum-dependent RIXS measurements were performed at resonant energies determined by the absorption peaks in XAS at a temperature of 20 K, with the exit slit opening to 40 μm corresponding to an average energy resolution of 53 meV (FWHM). To maximixe the CDW signal we used σ polarisation and a grazing-out geometry ($\theta>\Omega/2$). L-dependent RIXS measurements were performed by positioning the spectrometer arm at different Ω angles such that CDW was always centred at $H=0.333$ r.l.u.

Data fitting. RIXS data were normalized to incident photon flux, and subsequently corrected for self-absorption effects before fitting. Energy calibration was obtained by fitting the quasi-elastic peak to a pseudo-voigt function with width fixed to instrument resolution and setting the centre of the peak to $E=0$. The quasi-elastic peak intensities presented throughout the text were calculated by integration of RIXS spectra in the range $[-27, 27]$meV.

The H dependence of the quasi-elastic peak intensity was fitted to a Lorentzian peak shape atop a linear background. The in-plane correlation length is defined as $\xi_H=1/\Gamma$ at the condition of $\Omega=154°$, where $\Gamma=$HWHM is the scale parameter of the fitted Lorentzian. Note that ξ_H may not be equal but should be comparable to the absolutely genuine correlation length of the CDW object because its entire 3D shape is unknown. To convert from Å^{-1} to r.l.u., we used the STO lattice parameter $a=3.91$ Å. Temperature dependence of the integrated CDW intensity was fitted to an exponential function of the form $I(T;a,b,c)=a\exp(-bT)+c$. The $1/e^2$ intensity was $2/b$.

XAS data were normalized to incident photon flux, and then pre-L_3-edge intensity was aligned to zero with a fixed intensity at the post edge for all samples. XAS were collected up to the L_2 edge and the I_c projection was normalized to I_{ab} by scaling L_3 post edge intensity by a constant factor, minimizing the difference in intensity by least squares.

The features of the L_3 edge peak and post edge were fitted with four Gaussian peaks and an arctan step function. The centres of the peaks were fixed at approximately 852.2, 852.8, 853.7 and 856.3 eV and the step was fixed at 860.7 eV. Small changes were allowed in the peak centre between samples to improve the reduced χ^2, but were fixed between polarisations of the same sample. From left to right of each XAS spectrum, the width of the first two Gaussians was fixed to each other while that of the final Gaussian and step were fixed to each other. All other parameters were left floating. The peaks of interest were centred around ~852.2 and 852.8 eV. We assigned the lower energy peak to one from Nd–Ni hybridization and the higher one to the Ni^{1+} $2p\rightarrow 3d$ transition. Nd 5d and Ni 3d orbital contents were calculated by taking the ratio fitted peak intensities of the out-of-plane XAS and total fitted peak intensity of both projections—that is, orbital content $=I_c/(I_c+I_{ab})$. This was done for the Nd–Ni hybridized peak and Ni L_3 peak separately to determine Nd $5d_{3z^2-r^2}$ and Ni $3d_{3z^2-r^2}$ orbital content, respectively.

Data availability

All data supporting the findings of this study are available in the Supplementary Information and are deposited in the Zenodo repository at https://doi.org/10.5281/zenodo.6778273. Further information is available from the corresponding authors on reasonable request.

References

31. Ding, X. et al. Stability of superconducting Nd0.8Sr0.2NiO2 thin films. *Sci. China: Phys. Mech. Astron.* **65**, 267411 (2022).
32. Lee, K. et al. Aspects of the synthesis of thin film superconducting infinite-layer nickelates. *APL Mater.* **8**, 041107 (2020).
33. Zhou, K.-J. et al. I21: an advanced high-resolution resonant inelastic X-ray scattering beamline at Diamond Light Source. *J. Synchrotron Radiat.* **29**, 563–580 (2022).

Acknowledgements

We thank M. Dean and W.-S. Lee for insightful discussions. All data were taken at the I21 RIXS beamline of Diamond Light Source (UK) using the RIXS spectrometer designed, built and owned by Diamond Light Source. We thank Diamond Light Source for providing beamtime under proposal ID NT30296. We acknowledge T. Rice for technical support throughout the experiments. C.C.T. acknowledges funding from Diamond Light Source and the University of Bristol under joint doctoral studentship no. STU0372. L.Q. and H.L. acknowledge support from NSFC (grant nos. 11774044, 52072059 and 11822411) and SPRP-B of CAS (grant no. XDB25000000). K.-J.Z. and H.L. acknowledge support from NSF of Beijing (grant no. JQ19002).

Author contributions

K.-J.Z. conceived and supervised the project. C.C.T., J.C., K.-J.Z., S.A., M.G.-F. and A.N. performed XAS and RIXS measurements. C.C.T., J.C. and K.-J.Z. analysed RIXS data. L.Q., X.D. and L.H. synthesized and characterized thin film samples. M.W. and P.G. performed STEM measurements. All authors contributed to the discussion and interpretation of results. K.-J.Z., C.C.T. and J.C. wrote the manuscript with comments from all authors.

Competing interests

The authors declare no competing interests.

Additional information

Supplementary information The online version contains supplementary material available at https://doi.org/10.1038/s41563-022-01330-1.

Correspondence and requests for materials should be addressed to Liang Qiao or Ke-Jin Zhou.

Peer review information *Nature Materials* thanks the anonymous reviewers for their contribution to the peer review of this work.